Iterative method for optimal design of flat-spectral-response arrayed waveguide gratings

Shin-Woong Park,[1] Yohan Park,[2] Yun Yi,[2] and Hwi Kim[2,*]

[1]Center for Advanced Photovoltaic Materials, Korea University, 2511 Sejong-ro, Sejong City 339-700, South Korea

[2]Department of Electronics and Information Engineering, Korea University, 2511 Sejong-ro, Sejong City 339-700, South Korea

*Corresponding author: hwikim@korea.ac.kr

Received 22 May 2013; revised 10 September 2013; accepted 25 September 2013; posted 25 September 2013 (Doc. ID 190988); published 16 October 2013

A novel iterative projection-type optimal design algorithm of arrayed waveguide gratings (AWGs) with a flat spectral response is proposed based on the Fourier optics model of AWG. The enhancement of the spectral-response flatness of the AWG is demonstrated, with an analysis on the trade-off relationship between band flatness and crosstalk.

OCIS codes: (230.7390) Waveguides, planar; (070.0070) Fourier optics and signal processing; (230.1950) Diffraction gratings.

http://dx.doi.org/10.1364/AO.52.007295

1. Introduction

During the past three decades, arrayed waveguide gratings (AWGs), which spatially separate and combine wavelength channels, have been established as one of the key components of wavelength division multiplexing (WDM) optical networks [1]. Theoretical modeling and optimal design of AWG structure are important topics. The mathematical models of AWGs based on Fourier optics have become the preferred model choices for very simple and accurate means of simulating main device characteristics [2–4]. Furthermore, the accurate mathematical model can provide the merit function for the specified optimization algorithm. In this case, the AWG design can be formulated as a numerical optimization problem of AWG structural parameters. The use of a genetic algorithm for the optimal design of AWG, particularly having a flat spectral response, was reported [5].

Among several design considerations, the flat spectral response is a necessary requirement for multichannel AWGs to maximize the AWG performance. Several methods to flatten the spectral passbands have been addressed with multimode output waveguides [6], multimode interference coupler [7], multi-Rowland-circle structure [8], and multiple gratings [9] in the AWG design. In the previous research, we can find the common principle that the superposition and spatial average of the Gaussian spectral responses can lead to a desired flattened spectral response. Two or a few nonflattened spectral responses of the partial AWGs with a conventional form were superposed to effectively flat the spectral response in [6–9].

In this paper, the optimal AWG design problem is addressed, and a novel iterative projection-type method is proposed for optimal design of the AWGs with a flat spectral response. For this, the Fourier optics model of the spectral response of the AWG is mathematically modeled, and, within the framework, the optimal design strategy for obtaining spectral flat response is devised. We consider the lengths of the elementary waveguides of the AWG as the design variables and try to optimize the AWG structure. The aforementioned previous approaches can be understood as indirect design methods of taking the superposition of

1559-128X/13/307295-07$15.00/0

diffraction fields generated by partial AWGs designed by classical design formulas. But the proposed method in this paper is the nonlinear optimization aimed to the optimal profile of the AWG, which is the main contrast point from the previous works.

In Section 2, the Fourier optics model of AWG spectral response is established with numerical simulations. In Section 3, the projection-type iterative optimization algorithm is proposed for enhancing spectral-response flatness and is followed by concluding remarks.

2. Fourier Optics Model of AWG

In this section, two-dimensional (2D) Fourier optics model of AWG is developed. The AWG operation and spectral response are demonstrated based on the developed model. Figure 1 shows a schematic of $2M+1$ channel AWG with $2N+1$ waveguide array. In the input slab x' plane, the optical field at the center input port, $F(x';\lambda_s)$, is simply modeled as

$$F(x';\lambda_s) = \mathrm{rect}\left[\frac{x'-a}{w_{\mathrm{in}}}\right], \tag{1}$$

where w_{in} and a are the waveguide width and the spatial shift. λ_s is the operating wavelength in the slab waveguide of the AWG.

The optical field radiated from the input port propagates toward the waveguide array in the u' plane. The optical field distribution in the u' plane, $V(u';\lambda_s)$, is represented by the Fresnel transform of $F(x';\lambda_s)$ as

$$\begin{aligned} V(u';\lambda_s) &= \frac{e^{j2\pi f_{\mathrm{in}}/\lambda_s}}{\sqrt{j\lambda_s f_{\mathrm{in}}}} \int_{-\infty}^{\infty} F(x') \exp\left(-j\frac{2\pi}{\lambda_s f_{\mathrm{in}}} x'u'\right) \mathrm{d}x' \\ &= \frac{e^{j2\pi f_{\mathrm{in}}/\lambda_s}}{\sqrt{j\lambda_s f_{\mathrm{in}}}} \int_{-w_{\mathrm{in}}/2}^{w_{\mathrm{in}}/2} \exp\left(-j\frac{2\pi}{\lambda_s f_{\mathrm{in}}} x'u'\right) \\ &\quad \times \exp\left(-j\frac{2\pi}{\lambda_s f_{\mathrm{in}}} au'\right) \mathrm{d}x' \\ &= \frac{e^{j2\pi f_{\mathrm{in}}/\lambda_s}}{\sqrt{j\lambda_s f_{\mathrm{in}}}} w_{\mathrm{in}} \,\mathrm{sinc}\left(\frac{w_{\mathrm{in}}u'}{f_{\mathrm{in}}\lambda_s}\right) \exp\left(-j\frac{2\pi}{\lambda_s f_{\mathrm{in}}} au'\right), \end{aligned} \tag{2}$$

where f_{in} is the radius of the input channel waveguide array. The main lobe width of the sinc function

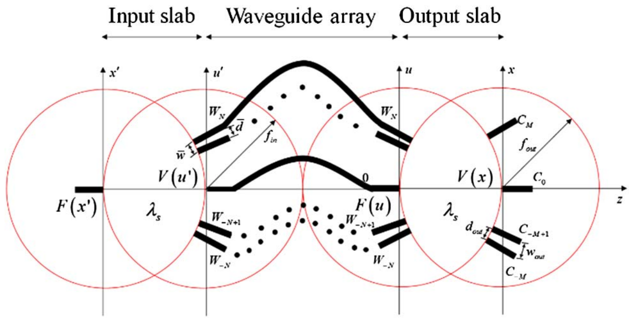

Fig. 1. Schematic of a two-dimensional AWG.

in $V(u';\lambda_s)$ is given by $2f_{\mathrm{in}}\lambda_s/w_{\mathrm{in}}$. It is assumed that the input waveguide array in the u' plane is within the main lobe area. Thus the total width of the input waveguide array is assumed to be given by

$$T_{\mathrm{in}} = \frac{2f_{\mathrm{in}}\lambda_s}{w_{\mathrm{in}}} q, \tag{3a}$$

where q is a number of $0 < q \le 1$. The waveguide array is assumed to be composed of $2N+1$ waveguides, with a uniform interval. The interval between two adjacent waveguides is

$$\bar{d} = \frac{2f_{\mathrm{in}}\lambda_s q}{w_{\mathrm{in}}(2N+1)}, \tag{3b}$$

and the waveguide fill factor is ρ, then the waveguide width is $\bar{w} = \rho\bar{d}$. The optical field at the u' plane, $V(u';\lambda_s)$, is delivered to the output ports at the u plane, through the waveguide array. The optical field, $F(u;\lambda_s)$, is represented as

$$F(u;\lambda_s) = \sum_{k=-N}^{N} A_k \,\mathrm{rect}\left[\frac{u-k\bar{d}}{\bar{w}}\right] \exp\left(-j\frac{2\pi}{\lambda_s f_{\mathrm{in}}} k\bar{d}a\right), \tag{4}$$

where A_k is the phase modulation imposed by the length of the kth waveguide. The sinc amplitude envelop in Eq. (2) is assumed to be approximately flat in the formulation of Eq. (4). $F(u;\lambda_s)$ propagates through the slab waveguide space to be coupled to one of $2M+1$ output channel waveguides at the x plane, which are denoted by $C_{-M}, C_{-M+1}, \ldots,$ and C_M.

The optical field, $V(x;\lambda_s)$, at the output channel in the x plane is represented by the optical Fourier transform of $F(u;\lambda_s)$, represented as

$$\begin{aligned} V(x;\lambda_s) &= \frac{e^{j2\pi f_{\mathrm{out}}/\lambda_s}}{\sqrt{j\lambda_s f_{\mathrm{out}}}} \left\{ \sum_{k=1}^{N} A_k \exp\left[-j\frac{2\pi}{\lambda_s f_{\mathrm{out}}} x(k\bar{d})\right] \bar{w} \right. \\ &\quad \times \mathrm{sinc}\left(\frac{\bar{w}x}{f_{\mathrm{out}}\lambda_s}\right) \exp\left(-j\frac{2\pi}{\lambda_s f_{\mathrm{in}}} k\bar{d}a\right) \\ &\quad + A_0 \bar{w}\,\mathrm{sinc}\left(\frac{\bar{w}x}{f_{\mathrm{out}}\lambda_s}\right) + \sum_{k=-N}^{-1} A_k \\ &\quad \times \exp\left[-j\frac{2\pi}{\lambda_s f_{\mathrm{out}}} x(k\bar{d})\right] \bar{w}\,\mathrm{sinc}\left(\frac{\bar{w}x}{f_{\mathrm{out}}\lambda_s}\right) \\ &\quad \left. \times \exp\left(-j\frac{2\pi}{\lambda_s f_{\mathrm{in}}} k\bar{d}a\right) \right\} \\ &= \frac{e^{j2\pi f_{\mathrm{out}}/\lambda_s}}{\sqrt{j\lambda_s f_{\mathrm{out}}}} \bar{w}\,\mathrm{sinc}\left(\frac{\bar{w}x}{f_{\mathrm{out}}\lambda_s}\right) \left[\sum_{k=-N}^{N} A_k \right. \\ &\quad \left. \times \exp\left[-j\frac{2\pi}{\lambda_s f_{\mathrm{out}}} x(k\bar{d})\right] \exp\left(-j\frac{2\pi}{\lambda_s f_{\mathrm{in}}} k\bar{d}a\right) \right] \\ &= \frac{e^{j2\pi f_{\mathrm{out}}/\lambda_s}}{\sqrt{j\lambda_s f_{\mathrm{out}}}} \bar{w}\,\mathrm{sinc}\left(\frac{\bar{w}x}{f_{\mathrm{out}}\lambda_s}\right) \left[\sum_{k=-N}^{N} A_k \right. \\ &\quad \left. \times \exp\left[-j\frac{2\pi}{\lambda_s f_{\mathrm{out}}} \left(x + \frac{f_{\mathrm{out}}}{f_{\mathrm{in}}} a\right)(k\bar{d})\right] \right]. \end{aligned} \tag{5}$$

The first sinc function constraints the envelop of $V(x;\lambda_s)$ by the finite width of $2\lambda_s f_{\rm out}/\bar{w}$, and the second term represents the periodic interference pattern, with a period of

$$T_{\rm out} = \frac{\lambda_s f_{\rm out}}{\bar{d}}. \tag{6a}$$

Here it is assumed that the main lobe width is equally divided and allowed to $(2M+1)$ equally separated output channel waveguides. The total width of the $(2M+1)$ output channel waveguide array is assumed to be equal to $T_{\rm out}$, then $T_{\rm out}$ is given by

$$T_{\rm out} = (2M+1)d_{\rm out} = \frac{\lambda_s f_{\rm out} w_{\rm in}(2N+1)}{2f_{\rm in}\lambda_s q}, \tag{6b}$$

where $d_{\rm out}$ is the interval of the adjacent output channel waveguides, and the second equality is obtained by plugging Eq. (3b) into Eq. (6a). The periodicity with the period of $T_{\rm out}$ is the operational mechanism of the cyclic operation of the AWG.

Let the parameter q in Eq. (6b) be 1, then the waveguide width $w_{\rm in}$ is given for $d_{\rm out}$ by

$$w_{\rm in} = \frac{2f_{\rm in}(2M+1)}{f_{\rm out}(2N+1)}d_{\rm out}. \tag{7}$$

Next let us consider the operation of the designed AWG for the operating wavelength of λ_w is the kth waveguide. Let us express the complex amplitude on the output port of the kth waveguide, A_k, in Eq. (4) as

$$A_k(\lambda_w) = \eta_k(\lambda_w)\exp(j\phi_k(\lambda_w)), \tag{8a}$$

where $\eta_k(\lambda_w)$ and $\phi_k(\lambda_w)$ are the amplitude and phase modulation of the kth waveguide, respectively. The phase modulation can be further decomposed as

$$\exp(j\phi_k(\lambda)) = \exp\left(j\frac{2\pi L}{\lambda_w}k\right)\exp\left(j\frac{2\pi}{\lambda_w}L_k\right). \tag{8b}$$

In conventional design, the parameter L is the length of the waveguide giving equal phase modulation for the design center wavelength $\bar{\lambda}_w$, $L = \bar{\lambda}_w m$, and the total length of the kth waveguide is tuned to the multiples of $L = \bar{\lambda}_w m$, as $Lk = \bar{\lambda}_w mk$. L_k is the optional length of the kth waveguide length.

In this paper, the optional parameters, $L_k(k = -M \sim M)$, are adopted as the extra design parameters to be optimized. In the next section, the iterative projection optimization algorithm of the tuning parameters, L_k, is proposed.

Here, before delving into the optimization algorithm, first consider the conventional AWG design with equal delay, $L_k = 0$. By substituting Eq. (8a) into Eq. (5), we can see that the optical field distribution at the x plane, $V(x;\lambda_s)$, is manipulated as

$$\begin{aligned}
V(x;\lambda_s) &= \frac{e^{j2\pi f_{\rm out}/\lambda_s}}{\sqrt{j\lambda_s f_{\rm out}}}\bar{w}\,\mathrm{sinc}\left(\frac{\bar{w}x}{f_{\rm out}\lambda_s}\right)\left[\sum_{k=-N}^{N}A_k\right.\\
&\quad\left.\times\exp\left[-j\frac{2\pi}{\lambda_s f_{\rm out}}x(k\bar{d})\right]\exp\left(-j\frac{2\pi}{\lambda_s f_{\rm in}}k\bar{d}a\right)\right]\\
&= \frac{e^{j2\pi f_{\rm out}/\lambda_s}}{\sqrt{j\lambda_s f_{\rm out}}}\bar{w}\,\mathrm{sinc}\left(\frac{\bar{w}x}{f_{\rm out}\lambda_s}\right)\left[\sum_{k=-N}^{N}\eta_k\right.\\
&\quad\left.\times\exp\left(j\frac{2\pi L}{\lambda_w}k\right)\exp\left[-j\frac{2\pi}{\lambda_s f_{\rm out}}\left(x+\frac{f_{\rm out}}{f_{\rm in}}a\right)(k\bar{d})\right]\right]\\
&= \frac{e^{j2\pi f_{\rm out}/\lambda_s}}{\sqrt{j\lambda_s f_{\rm out}}}\bar{w}\,\mathrm{sinc}\left(\frac{\bar{w}x}{f_{\rm out}\lambda_s}\right)\left[\sum_{k=-N}^{N}\eta_k\right.\\
&\quad\times\exp\left(j\frac{2\pi\bar{\lambda}_w m}{\lambda_w}k\right)\\
&\quad\left.\times\exp\left[-j\frac{2\pi}{\lambda_s f_{\rm out}}\left(x+\frac{f_{\rm out}}{f_{\rm in}}a\right)(k\bar{d})\right]\right]\\
&= \frac{e^{j2\pi f_{\rm out}/\lambda_s}}{\sqrt{j\lambda_s f_{\rm out}}}\bar{w}\,\mathrm{sinc}\left(\frac{\bar{w}x}{f_{\rm out}\lambda_s}\right)\left[\sum_{k=-N}^{N}\eta_k\right.\\
&\quad\left.\times\exp\left[-j\frac{2\pi}{\lambda_s f_{\rm out}}\left(x+\frac{f_{\rm out}}{f_{\rm in}}a-\frac{\bar{\lambda}_w m\lambda_s f_{\rm out}}{\lambda_w\bar{d}}\right)(k\bar{d})\right]\right].
\end{aligned} \tag{9}$$

For convenience, let the spatial shift of the input channel waveguide be set to $a = 0$. $V(x;\lambda_s)$ is obtained as

$$\begin{aligned}
V(x;\lambda_s) &= \frac{e^{j2\pi f_{\rm out}/\lambda_s}}{\sqrt{j\lambda_s f_{\rm out}}}\bar{w}\,\mathrm{sinc}\left(\frac{\bar{w}x}{f_{\rm out}\lambda_s}\right)\left[\sum_{k=-N}^{N}\eta_k\right.\\
&\quad\left.\times\exp\left[-j\frac{2\pi}{\lambda_s f_{\rm out}}\left(x-\frac{\bar{\lambda}_w m\lambda_s f_{\rm out}}{\lambda_w\bar{d}}\right)(k\bar{d})\right]\right].
\end{aligned} \tag{10}$$

The peak intensity point in the optical field distribution is dependent of the operating wavelength λ_w, found with the following condition,

$$\frac{2\pi}{\lambda_s f_{\rm out}}\left(x-\frac{\bar{\lambda}_w m\lambda_s f_{\rm out}}{\lambda_w\bar{d}}\right)\bar{d} = 2\pi p, \tag{11a}$$

where p is an integer. The peak position, i.e., focal position, at the output channel plane, is obtained as

$$\begin{aligned}
x &= \frac{p\lambda_s f_{\rm out}}{\bar{d}} + \frac{\bar{\lambda}_w m\lambda_s f_{\rm out}}{\lambda_w\bar{d}} = \frac{\lambda_s f_{\rm out}}{\bar{d}}\left(p+\frac{\bar{\lambda}_w m}{\lambda_w}\right)\\
&= \frac{\lambda_s f_{\rm out}}{\bar{d}}\left(p+m-\frac{\Delta\lambda_w m}{\bar{\lambda}_w+\Delta\lambda_w}\right) = \frac{\lambda_s f_{\rm out}}{\bar{d}}\left(p+m-\frac{\Delta\lambda_w m}{\lambda_w}\right)\\
&= \frac{\lambda_s f_{\rm out}}{\bar{d}}(p+m) - \frac{f_{\rm out}n_w\Delta\lambda_w m}{\bar{d}}\\
&= \frac{\lambda_s f_{\rm out}}{\bar{d}}(p+m) - \frac{f_{\rm out}\Delta\lambda_s m}{\bar{d}},
\end{aligned} \tag{11b}$$

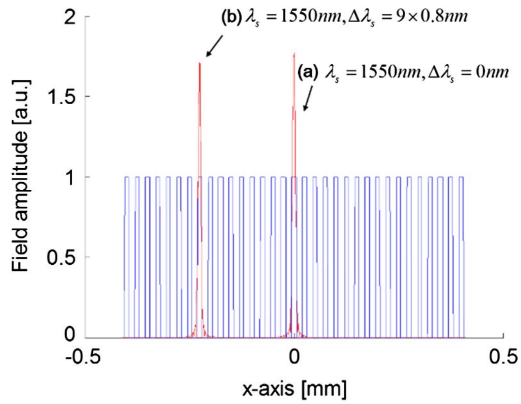

Fig. 2. Diffraction field profile $V(x;\lambda_s)$: (a) $\lambda_s = 1550$ nm, $\Delta\lambda_s = 0$ nm and (b) $\lambda_s = 1550$ nm, $\Delta\lambda_s = 9\times 0.8$ nm.

where the waveguide wavelength λ_w is assumed to be $\lambda_w = n_w\lambda_s$. n_w is the effective refractive index of the waveguide. In Eq. (11b), it is manifested that the peak position translation is due to the wavelength spacing $\Delta\lambda_s$. In the design of AWG, the peak position translation due to the wavelength is accurately controlled to be equal to the output waveguide channel interval d_{out}, such that $d_{\text{out}} = f_{\text{out}}\Delta\lambda_s m/\bar{d}$.

Following the above theory, we designed the 33 channel numbers, 0.8 nm channel spacing, center wavelength 1550 nm, cyclic operation, and symmetric (equal focal lengths) AWG. Let us consider the symmetric type AWG with $f_{\text{in}} = f_{\text{out}}$, then the width of the input port waveguide, w_{in}, is obtained by $w_{\text{in}} = [2(2M+1)/(2N+1)]d_{\text{out}} = 0.4d_{\text{out}}$. If we want to make 33 channels AWG ($2M+1 = 33$) with the number of waveguides, $2N+1$, 165, w_{in}, and d_{out} are determined to be 10 and 25 μm, respectively. The period of the cyclic operation of Eq. (6b) is $T_{\text{out}} = 825$ μm. The interval between two adjacent waveguides, $\bar{d}$, of Eq. (3b) is obtained by $\bar{d} = [2f_{\text{in}}\lambda_s q/w_{\text{in}}(2N+1))] = 21.3$ μm for the center wavelength $\lambda_s = 1550$ nm. For the aforementioned design parameters, $\bar{d} = 21.3$ μm, $d_{\text{out}} = 25$ μm, $\Delta\lambda_s = 0.8$ nm, and $f_{\text{out}}m = 0.665625$ are obtained. We set $f_{\text{out}} = 0.01128177966102$ and $m = 59$.

Figure 2 shows the diffraction field profile $V(x;\lambda_s)$, and the wavelength switching of the peak intensity position. Figures 2(a) and 2(b) are the diffraction field profiles for $\lambda_s = 1550$ nm and $\lambda_s = 1550$ nm $+ 9\times 0.8$ nm, respectively. The peak positions for the wavelengths of $\lambda_s = 1550$ nm and $\lambda_s = 1550$ nm $+ 9\times 0.8$ nm are tuned to the central waveguide and the leftward ninth waveguide, respectively.

The diffraction field $V(x;\lambda_s)$ is coupled to the output channel waveguides. The coupling power is calculated by the overlap integral of $V(x;\lambda_s)$ and the kth output waveguide channel given by $W_k(x) = \text{rect}[(x - kd_{\text{out}})/w_{\text{out}}]$, which is represented by

$$C_k(\lambda_s) = \int V(x;\lambda_s)W_k(x)\mathrm{d}x. \tag{12}$$

In Fig. 3, the transmission spectra of all 33 channels with the wavelength range from 1537.2 to 1562.8 nm with the channel spacing of 0.8 nm, $\sum_{k=-M}^{M} C_k(\lambda_s)$, are plotted. On the basis of definition for flatness and crosstalk in Fig. 4, the crosstalk and flatness of the spectral response are estimated as −5 dB and −0.5 dB in Fig. 3, respectively.

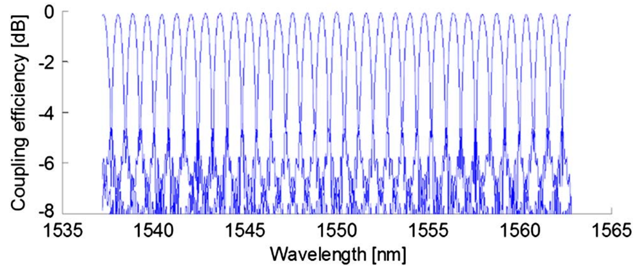

Fig. 3. Transmission spectra of all 33 channels with the wavelength ranging from 1520 to 1580 nm and the channel spacing of 0.8 nm.

3. Iterative Method for Optimizing Extra-Phase Freedom

To improve or modify the spectral response of the AWG, we need to design extra-phase freedom (extra-length freedom) of the kth waveguide, ΔL_k, for shaping the complex field pattern $V(x;\lambda_s)$. Inserting ΔL_k into the model of Eq. (9), we can represent $V(x;\lambda_s)$ as

$$V(x) = \sum_{k=-N}^{N} G_k(x)\eta_k \exp\left(j\frac{2\pi\Delta L_k}{\lambda_w}\right), \tag{13a}$$

where $G_k(x)$ is the AWG response function for the complex modulation caused by the extra phase freedom

$$G_k(x) = \frac{e^{j2\pi f_{\text{out}}/\lambda_s}}{\sqrt{j\lambda_s f_{\text{out}}}}\bar{w}\,\text{sinc}\left(\frac{\bar{w}x}{f_{\text{out}}\lambda_s}\right) \times \exp\left[-j\frac{2\pi}{\lambda_s f_{\text{out}}}\left(x - \frac{\bar{\lambda}_w m\lambda_s f_{\text{out}}}{\lambda_w\bar{d}}\right)(k\bar{d})\right]. \tag{13b}$$

Let $\phi_k = (2\pi\Delta L_k)/\lambda_w$ and discretize Eq. (13a) as the following $(2N+1)\times(2N+1)$ matrix equation:

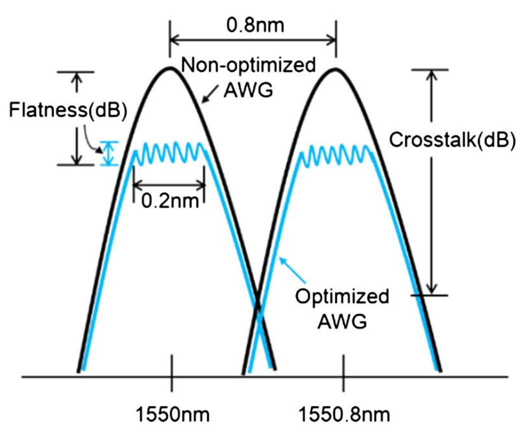

Fig. 4. Schematic of crosstalk and flatness level in optimized AWG.

$$\begin{bmatrix} V_{-N} \\ \vdots \\ V_0 \\ \vdots \\ V_N \end{bmatrix} = \begin{bmatrix} G_{-N,-N} & \cdots & G_{0,-N} & \cdots & G_{N,-N} \\ \vdots & \ddots & & & \\ G_{-N,-N} & & G_{0,-N} & & G_{N,-N} \\ \vdots & & & \ddots & \\ G_{-N,-N} & & G_{0,-N} & & G_{N,-N} \end{bmatrix} \begin{bmatrix} \eta_{-N}\exp(j\phi_{-N}) \\ \vdots \\ \eta_0 \exp(j\phi_0) \\ \vdots \\ \eta_N \exp(j\phi_N) \end{bmatrix}, \tag{14}$$

where V_n is the value of $V(x)$ at $x = x_n$. η_k and ϕ_n are the values of the amplitude and phase of the complex optical field at the input waveguide. The task is to find the optimal ΔL_k for shaping V_n. A projection-type iterative algorithm is devised to optimize the extra-phase freedom ΔL_k in Eq. (14).

In Fig. 5, a schematic diagram of the proposed iterative projection algorithm is presented. This optimization process is inspired from the iterative Fourier transform algorithm (IFTA) used in the optimal design of diffractive optical element [10,11]. The ideal goal of this design is to obtain a flat spectral response at the output port. For this, the target intensity profile is taken by the form $I(x)$ shown in Fig. 6. In the algorithm diagram in Fig. 5, the forward transform between the input waveguide plane and the output waveguide is described by **G**. For iterative optimization, the inverse transform is necessary, which is simply defined by $\mathbf{G}^{-1}$, the inverse matrix of **G**.

At the first step, for the desired amplitude pattern, $I(x)$, the diffraction field $V(x)$ is updated to $\bar{V}(x)$:

$$\bar{V}(x) = \begin{cases} \eta V(x) & \text{for } I(x) = 0 \\ I(x)\exp(j\measuredangle V(x)) & \text{for } I(x) \neq 0 \end{cases}. \tag{15}$$

The complex field at the input wave plane is obtained by the inverse transform of $\bar{V}(x)$:

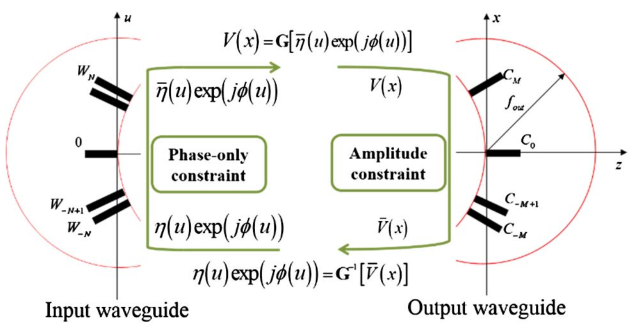

Fig. 5. Iterative projection algorithm.

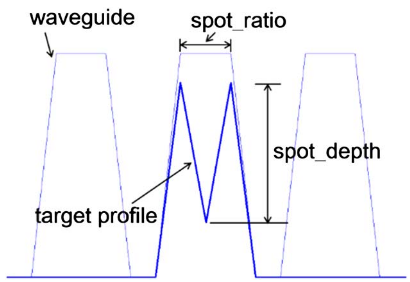

Fig. 6. Target amplitude profile for iterative projection algorithm with two variables: spot ratio and spot depth.

$$\eta(u)\exp(j\phi(u)) = \mathbf{G}^{-1}(\bar{V}(x)), \tag{16}$$

where $\eta(u)$ and $\exp(j\phi(u))$ are the amplitude and phase profiles of the complex field in the u plane. At the second step, the amplitude profile is clipped to a predefined profile; for example, a constant. The obtained phase profile $\phi(u)$ is an updated phase profile that has approached closer to the optimum solution. The diffraction field distribution at the output channel plane is gradually changed to be similar to the desired target amplitude profile.

For obtaining the response flatness, the target amplitude pattern is designed as shown in Fig. 6, with a reference image of the part of the output channel

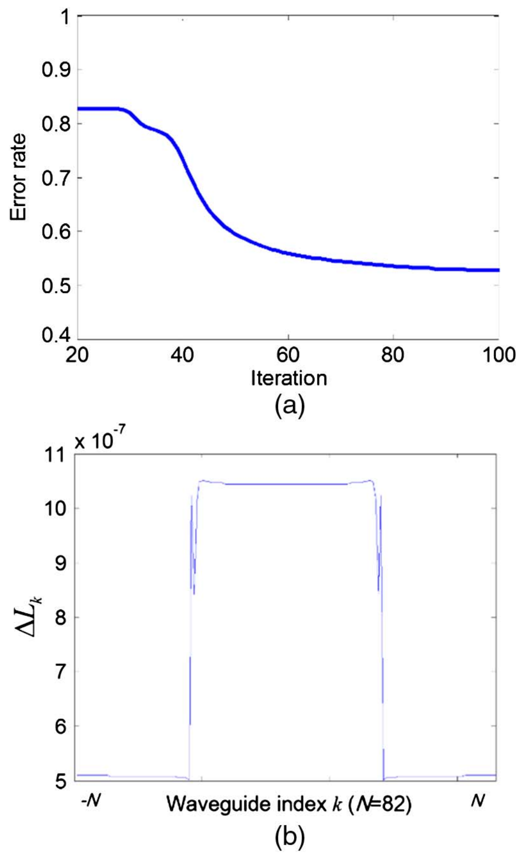

Fig. 7. (a) Convergence feature of the proposed iterative projection algorithm. (b) Optimal profile of the extra-phase freedom over 165 waveguide array.

waveguide array. The spot ratio and spot depth are the two designed parameters, by varying which we can control the levels of the crosstalk and the response flatness.

In Fig. 7, the design result is presented. In Fig. 7(a), the convergence graph of the RMS error of the obtained diffraction field amplitude and the target amplitude profile is plotted. The optimization was performed for the design center wavelength 1550 nm. In Fig. 7(b), the resultant extra-phase-freedom profile for a 165 waveguide array is presented. These results were calculated by the MATLAB simulation using 16-core workstation, with memory of 192 gigabytes (runtime is 5 min in total).

The diffraction patterns in the output plane $V(x;\lambda_s)$ for the design of center wavelength $\lambda_s = 1550$ nm and $\lambda_s = 1550\ \text{nm} + 9 \times 0.8$ nm are compared in Fig. 8(a) with the field profile of the conventional AWG with $\Delta L_k = 0$. In this case, the spot ratio and spot depth are set to 1.9 and 1.0, respectively. It is confirmed that the proposed iterative projection algorithm succeeds in shaping the desired feature in the diffraction field profile, and the diffraction field profile is almost conserved with wavelength switching ($\lambda_s = 1550\ \text{nm} + 9 \times 0.8$ nm). The undesired sidelobe profile is the by-product of the optimization. According to Eq. (12), the spectral response of the designed AWG is calculated and plotted in Fig. 8(b). The crosstalk and the flatness of the spectral response are estimated as −2.5 and −0.05 dB in Fig. 8(b), respectively.

Also it is seen that the diffraction effects impose a constraint of the trade-off between spectral response flatness and crosstalk level of the AWG. The proposed iterative optimization algorithm allows us to control the enhancement level of the spectral response flatness by tuning the spot ratio and spot depth. It is expected that the trade-off constraint can be relaxed and further optimized by application of more advanced optimization techniques [11].

Additional simulations to analyze the tolerance of the flatness to the deviation in the profile ΔL_k are performed. The deformed profile in the AWG is simply modeled as $\eta \Delta L_k$ [Fig. 9(a)], where the structural deviation parameter η is set up in the range of $0.5 \le \eta \le 1.5$. The case of $\eta = 1$ corresponds to the optimal profile ΔL_k. By changing the deviation parameter η, we profiled the spectral response of the AWGs with $\eta \Delta L_k$ in Fig. 9(b). It is seen that,

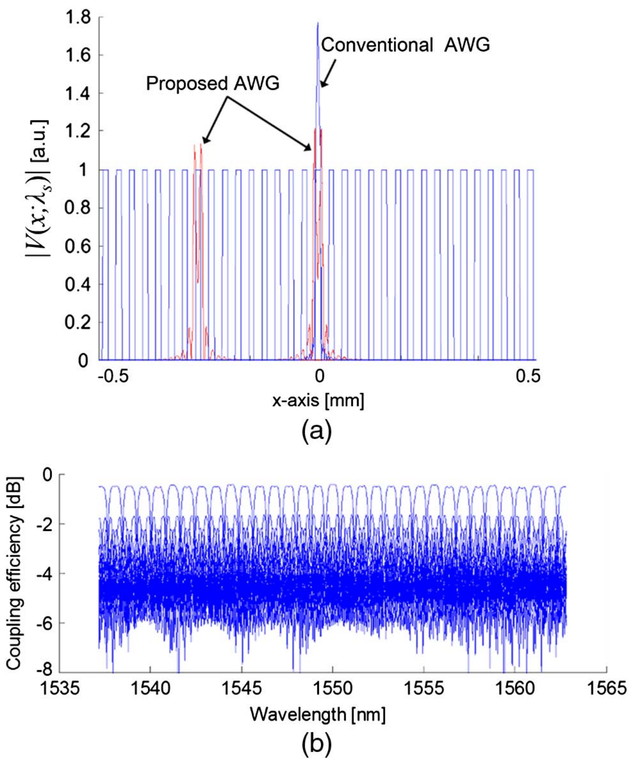

Fig. 8. (a) Comparison of the field profiles obtained by the conventional method and the proposed method. (b) Simulated spectral response of the designed AWG (crosstalk = −2.5 dB, flatness = −0.05 dB).

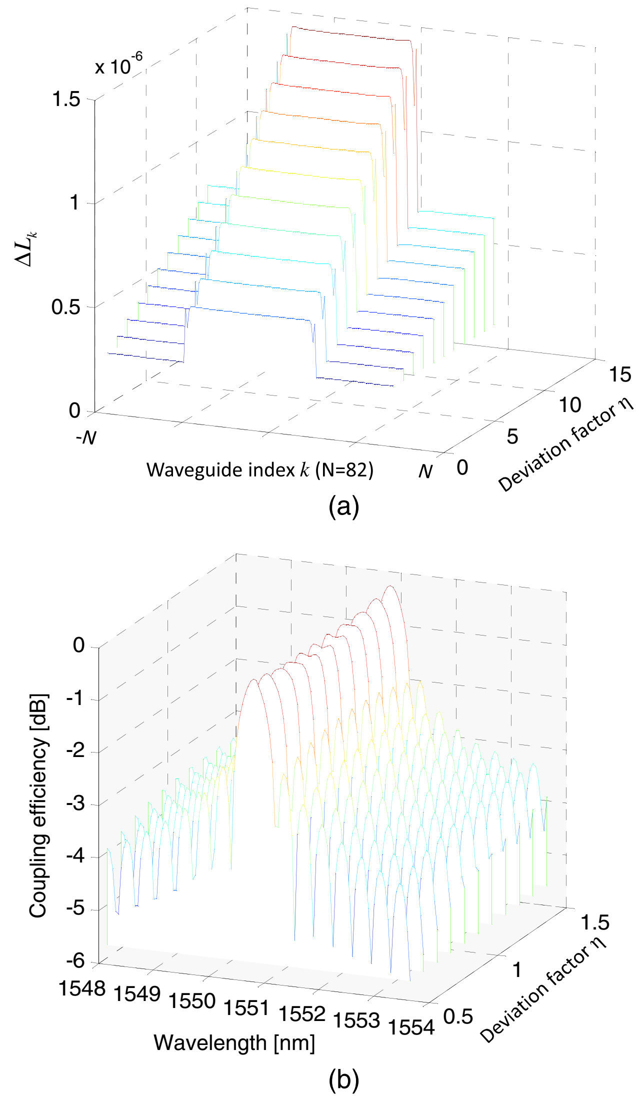

Fig. 9. Tolerance analysis: (a) ΔL_k profile with the deviation factor η and (b) spectral response variation with the deviation factor η.

for $0.75 \leq \eta \leq 1.25$, the flat-top feature is perceivable, but, in the other region of η, the flat-top features disappear in the spectral response. In the region of $0.75 \leq \eta \leq 1.25$, the variation in the crosstalk level is so small as to be negligible. In general, the crosstalk and flatness have a trade-off relationship, but, in accordance with this simulation, we can conclude that, within 25% tolerance margin of ΔL_k ($0.75 \leq \eta \leq 1.25$), the flatness and crosstalk are reliable.

4. Conclusion

We have proposed a fast and efficient iterative projection-type optimal design algorithm of an AWG with a flat spectral response and developed a Fourier optics model of the AWG. The optimization target function parameterized by spot ratio and spot depth has been devised for controlling the crosstalk and flatness in the spectral response.

This work was supported by a Korea University grant.

References

1. C. Brackett, "Dense wavelength division multiplexing networks: principles and applications," IEEE J. Sel. Areas Commun. **8**, 948–964 (1990).
2. A. S. Manouri and R. Faraji-Dana, "Arrayed waveguide grating multiplexers with flat spectral response using non-uniform arrays," *Proceedings of the 12th International Conference on Microelectronics*, Teheran (2000), pp. 307–310.
3. F. Xiao, G. Li, and A. Xu, "Modeling and design of irregularly arrayed waveguide gratings," Opt. Express **15**, 3888–3901 (2007).
4. I. Molina-Fernandez and J. G. Wanguemert-Perez, "Improved AWG Fourier optics model," Opt. Express **12**, 4804–4821 (2004).
5. P. Munoz and S. D. Walker, "Design of arrayed-waveguide gratings using hybrid Fourier–Fresnel transform techniques," IEEE J. Sel. Top. Quantum Electron. **5**, 1379–1384 (1999).
6. M. R. Amersfoort, C. R. de Boer, F. P. G. M. van Ham, M. K. Smit, P. Demeester, J. J. G. M. van der Tol, and A. Kuntze, "Phased-array wavelength demultiplexer with flattened wavelength response," Electron. Lett. **30**, 300–302 (1994).
7. M. R. Amersfoort, J. B. D. Soole, H. P. LeBlance, N. C. Andreadakis, A. Rajhel, and C. Caneau, "Passband broadening of integrated arrayed waveguide filters using multimode interference couplers," Electron. Lett. **32**, 449–451 (1996).
8. Y. P. Ho, H. Li, and Y. J. Chen, "Flat channel-passband-wavelength multiplexing and demultiplexing devices by multiple-Rowland-circle design," IEEE Photon. Technol. Lett. **9**, 342–344 (1997).
9. A. Rigny, A. Bruno, and H. Sik, "Multigrating method for flattened spectral response wavelength multi/demultiplexer," Electron. Lett. **33**, 1701–1702 (1997).
10. H. Kim and B. Lee, "Optimal non-monotonic convergence of iterative Fourier transform algorithm," Opt. Lett. **30**, 296–298 (2005).
11. H. Kim, B. Yang, and B. Lee, "Iterative Fourier transform algorithm with regularization for the optimal design of diffractive optical elements," J. Opt. Soc. Am. A **21**, 2353–2365 (2004).